



HAL
open science

Centroidal Trajectory Generation and Stabilization Based on Preview Control for Humanoid Multi-Contact Motion

Masaki Murooka, Mitsuharu Morisawa, Fumio Kanehiro

► **To cite this version:**

Masaki Murooka, Mitsuharu Morisawa, Fumio Kanehiro. Centroidal Trajectory Generation and Stabilization Based on Preview Control for Humanoid Multi-Contact Motion. *IEEE Robotics and Automation Letters*, 2022, 7 (3), pp.8225-8232. 10.1109/LRA.2022.3186515 . hal-03720407

HAL Id: hal-03720407

<https://cnrs.hal.science/hal-03720407>

Submitted on 12 Jul 2022

HAL is a multi-disciplinary open access archive for the deposit and dissemination of scientific research documents, whether they are published or not. The documents may come from teaching and research institutions in France or abroad, or from public or private research centers.

L'archive ouverte pluridisciplinaire **HAL**, est destinée au dépôt et à la diffusion de documents scientifiques de niveau recherche, publiés ou non, émanant des établissements d'enseignement et de recherche français ou étrangers, des laboratoires publics ou privés.

Centroidal Trajectory Generation and Stabilization based on Preview Control for Humanoid Multi-contact Motion

Masaki Murooka, Mitsuharu Morisawa and Fumio Kanehiro

Abstract—Multi-contact motion is important for humanoid robots to work in various environments. We propose a centroidal online trajectory generation and stabilization control for humanoid dynamic multi-contact motion. The proposed method features the drastic reduction of the computational cost by using preview control instead of the conventional model predictive control that considers the constraints of all sample times. By combining preview control with centroidal state feedback for robustness to disturbances and wrench distribution for satisfying contact constraints, we show that the robot can stably perform a variety of multi-contact motions through simulation experiments.

Index Terms—Humanoid and Bipedal Locomotion; Multi-Contact Whole-Body Motion Planning and Control.

I. INTRODUCTION

HUMANOID robots can perform locomotion and manipulation that maximize the potential of the high-degree-of-freedom body through multi-contact motion using not only the feet but also the hands. The planning and control of such multi-contact motion have been studied extensively in the last decade. In particular, many studies have focused on the robot centroidal dynamics [1] instead of the full dynamics, thereby reducing the dimensionality and computational cost [2], [3], [4]. However, even focusing on the centroidal dynamics, it is still non-trivial to realize receding horizon control that can be executed on the order of submillisecond due to its nonlinearity and contact constraints.

In this paper, we propose the centroidal online trajectory generation method based on preview control and the stabilization control method to compensate for the error of the centroidal state. The proposed method takes a new approach that is entirely different from model predictive control (MPC), which explicitly considers time series constraints [5], [6], [7], [8], [9], and has the advantage of significantly lowering computational costs. In the simulation experiments of humanoid multi-contact motion, our method can sequentially generate the centroidal trajectory with stabilization control within 1 ms, considering the reference input of the horizon of 2 s (400 sample points); to

the best of our knowledge, this is one of the fastest centroidal trajectory generation and control methods that can handle general multi-contact motion without relying on the biped-specific dynamics. The effectiveness of the proposed method is demonstrated through simulation experiments in which a humanoid robot performs various challenging dynamic multi-contact motions.

A. Related Works

1) *Centroidal Online Trajectory Generation*: By generating a centroidal trajectory with the receding horizon control scheme, the robot can robustly respond to environmental changes and tracking errors by flexibly modifying the position and timing of contact transitions [10]. MPC, which is formulated as a quadratic programming (QP) problem, has been widely used for the receding horizon control of legged robots [5], [6], [7], [8], [9]. In MPC, equality and inequality constraints including contact force constraints are imposed on all input / state variables of sampling times in the horizon. Therefore, the dimensionality of the constraints tends to be large, and it is not easy to solve it on the order of submillisecond, even with state-of-the-art QP solvers.

In this paper, we propose an application of preview control [11], which does not explicitly consider these constraints. Since the preview control requires only a single matrix multiplication at runtime and does not require an iterative computation, it is considerably faster than MPC, which requires solving a QP. We show that even though the constraints are omitted in the preview control, a realistic reference trajectory (but a fairly rough one that is discontinuous and non-differentiable) and post-processing wrench projection can generate feasible robot motions. We note that differential dynamic programming, which has recently been used for robot motion generation [12], can also be applied to fast unconstrained receding horizon control.

2) *Balance Stabilization Control*: Our proposed centroidal stabilization control is similar to the balance control [13] since it provides feedback on the centroidal position and orientation. However, our method differs in that the resultant wrench obtained from online trajectory generation is used for feedforward. While some stabilization control methods for multi-contact motion target specific tasks (e.g., ladder climbing [14] or whole-body pushing [15]), our method can handle various multi-contact motions including locomotion on flat ground, handrail stairs, and vertical ladders.

Manuscript received: February, 16, 2022; Revised May, 9, 2022; Accepted June, 23, 2022.

This paper was recommended for publication by Editor L. Pallottino upon evaluation of the Associate Editor and Reviewers' comments. This work was supported by KAKENHI (21H01300).

The authors are with CNRS-AIST JRL (Joint Robotics Laboratory), IRL and National Institute of Advanced Industrial Science and Technology (AIST), 1-1-1 Umezono, Tsukuba, Ibaraki 305-8560, Japan. {m-murooka, m.morisawa, f-kanehiro}@aist.go.jp

Digital Object Identifier (DOI): see top of this page.

For bipedal walking, stabilization control based on the divergent component of motion (DCM) has been widely proposed [16], [17]. Although this is a powerful method, it relies on the linear inverted pendulum mode (LIPM) [18], which assumes bipedal dynamics, and is difficult to extend to general multi-contact motion. In this paper, we show that the proposed centroidal control for multi-contact motion includes the proportional control of DCM for bipedal walking as a particular case, and derive the relationship between the gain parameters of the two controls.

B. Contributions of this Paper

The contributions of our work are threefold: (i) online generation method of robot centroidal trajectory with very low computational cost based on preview control, (ii) a control system that can handle humanoid bipedal walking and multi-contact motion including hand contacts without changing the parameters, (iii) showing that a humanoid robot can perform various challenging multi-contact motions such as handrail stairs and vertical ladders in simulation.

II. METHOD OVERVIEW

Fig. 1 shows the proposed control system for humanoid multi-contact motion. The control system consists mainly of centroidal online trajectory generation and stabilization control. These two modules are introduced in Sections III and IV, respectively, followed by simulation experiments in Section V.

We assume that the robot is joint position controlled. The sequence of contact positions \mathcal{C}^d of the hands and feet is assumed to be determined by a global planner [19], or manually.

III. CENTROIDAL ONLINE TRAJECTORY GENERATION

A. 6-DoF Centroidal Preview Control

1) *Approximated Centroidal Dynamics*: The centroidal dynamics of a humanoid robot are governed by the Newton-Euler equation [20]:

$$m\ddot{\mathbf{c}} = \mathbf{f} - m\mathbf{g} \quad (1a)$$

$$\dot{\mathbf{L}} = \mathbf{n} - \mathbf{c} \times \mathbf{f} \quad (1b)$$

$m \in \mathbb{R}$ is the robot mass. $\mathbf{c} \in \mathbb{R}^3$ is the robot CoM. $\mathbf{L} \in \mathbb{R}^3$ is the centroidal angular momentum around the CoM. $\mathbf{g} = [0 \ 0 \ g]^\top$ is the (vertical upward) gravitational acceleration vector. $\mathbf{f}, \mathbf{n} \in \mathbb{R}^3$ are the force and moment from the contacts between the robot and the environment, represented in world coordinates. Especially, \mathbf{n} is the moment around the world origin.

We introduce the resultant force and moment, which combines the effects of contacts and gravity, as follows:

$$\bar{\mathbf{f}} = \mathbf{f} - m\mathbf{g} \quad (2a)$$

$$\bar{\mathbf{n}} = \mathbf{n} - \mathbf{c} \times \mathbf{f} \quad (2b)$$

In the following, the symbols with bar denote the resultant force and moment combined with gravity.

2) *State Equation for Preview Control*: The linear components of centroidal dynamics (1a) are represented by the following state equations:

$$\dot{\mathbf{x}}_{L*} = \begin{bmatrix} 0 & 1 & 0 \\ 0 & 0 & 1 \\ 0 & 0 & 0 \end{bmatrix} \mathbf{x}_{L*} + \begin{bmatrix} 0 \\ 0 \\ 1 \end{bmatrix} u_{L*} \quad (3a)$$

$$\mathbf{y}_{L*} = \begin{bmatrix} 1 & 0 & 0 \\ 0 & 0 & m \end{bmatrix} \mathbf{x}_{L*} \quad (3b)$$

$$\begin{aligned} \text{where } \mathbf{x}_{L*} &= [c_* \ \dot{c}_* \ \ddot{c}_*]^\top \\ u_{L*} &= \ddot{c}_* \\ \mathbf{y}_{L*} &= [c_* \ \bar{\mathbf{f}}_*]^\top \\ * &\in \{x, y, z\} \end{aligned}$$

c_* and $\bar{\mathbf{f}}_*$ ($* \in \{x, y, z\}$) represent the axis components of \mathbf{c} and $\bar{\mathbf{f}}$, respectively. The states consist of the CoM position, velocity, and acceleration. The input is the CoM jerk. The outputs consist of the CoM and the resultant force.

Compared to the preview control for bipedal walking by Kajita et al. [21], the definitions of states and input are the same, but the definition of output is different. In bipedal walking [21], the ZMP is regarded as an output to follow the reference ZMP trajectory, whereas in our method, the CoM and the force are regarded as outputs to support general multi-contact motion. We chose this output definition from the consideration that the ZMP in bipedal walking has force information as the center of pressure and also has CoM information based on the CoM-ZMP relationship. One of the main contributions of this paper is that preview control with this output definition works effectively to generate general multi-contact motions.

3) *Optimal Input Calculation*: Given reference trajectories for the robot CoM and resultant force, the following objective function is minimized:

$$J_{L*} = \sum_{i=k}^{\infty} \left(\|\mathbf{y}_{L*}[i] - \mathbf{y}_{L*}^{\text{ref}}[i]\|_{\mathbf{Q}_L}^2 + \|u_{L*}[i]\|_{\mathbf{R}_L}^2 \right) \quad (4a)$$

$$= \sum_{i=k}^{\infty} \left(\left\| \begin{bmatrix} c_*[i] - c_*^{\text{ref}}[i] \\ \bar{\mathbf{f}}_*[i] - \bar{\mathbf{f}}_*^{\text{ref}}[i] \end{bmatrix} \right\|_{\mathbf{Q}_L}^2 + \|\ddot{c}_*[i]\|_{\mathbf{R}_L}^2 \right) \quad (4b)$$

\mathbf{Q}_L and \mathbf{R}_L are the objective weights of output and input, respectively. For a general vector \mathbf{x} , $\|\mathbf{x}\|_{\mathbf{W}}^2$ represents $\mathbf{x}^\top \mathbf{W} \mathbf{x}$ where \mathbf{W} is \mathbf{Q}_L or \mathbf{R}_L . k is the control step index. We always set the reference force to zero. The reference CoM trajectory was determined by simple rules such as the center of the contact points. See Section V for examples.

According to the preview control theory [11], the optimal input can be obtained as follows:

$$u_{L*}^{\text{opt}}[k] = -\mathbf{K}_{\text{fb}} \mathbf{x}_{L*}[k] + \sum_{i=1}^{N_h} \mathbf{K}_{\text{ff}}[i] \mathbf{y}_{L*}^{\text{ref}}[k+i] \quad (5)$$

N_h is the number of time-steps of the preview window. Since the state equation (3) depends only on the robot mass, the gains \mathbf{K}_{fb} and \mathbf{K}_{ff} are fixed as long as the robot mass is constant. See [11] and [21] for the derivation of these gain matrices. The equation (5) requires only matrix multiplication, which is considerably less computationally expensive than conventional

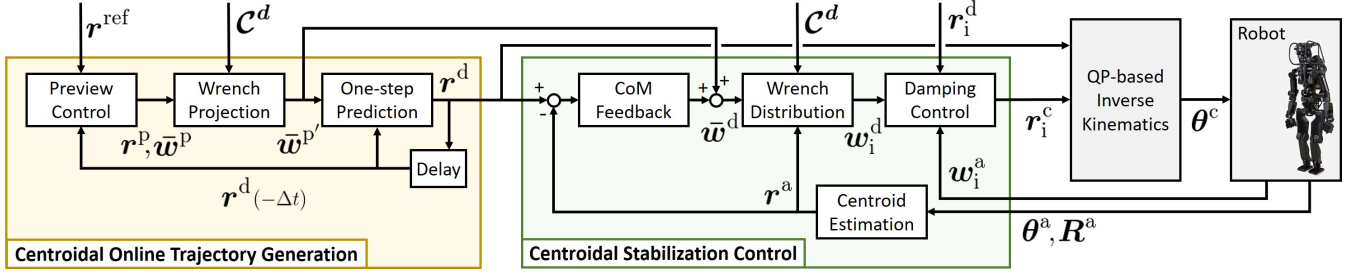


Fig. 1. Overall components of the control system for humanoid multi-contact motion.

multi-contact motion generation methods [19] such as MPC with constraints [5] or trajectory optimization [2]. Although our preview control does not consider constraints on contact forces, we show in Section V that a realistic reference trajectory (but a fairly rough one) and post-processing can produce feasible robot motions.

4) *6-DoF Trajectory Generation*: We approximate the centroidal angular momentum in (1b) as follows:

$$L = I_{\text{all}} \dot{q} \approx I_{\text{base}} \omega \approx I \omega \quad (6)$$

$\dot{q} \in \mathbb{R}^{N_q}$ is the joint velocity vector including the 6-DoF virtual joint velocity for the robot base link. $I_{\text{all}} \in \mathbb{R}^{3 \times N_q}$ is the angular part of the centroidal momentum matrix [1]. $\omega \in \mathbb{R}^3$ is the angular velocity of the base link. $I_{\text{base}} \in \mathbb{R}^{3 \times 3}$ is the block matrix of I_{all} corresponding to the base link angular velocity. $I \in \mathbb{R}^{3 \times 3}$ is a constant and diagonal approximation of I_{base} . The approximation in equation (6) assumes that (i) the angular momentum due to joint velocity is negligible, (ii) I_{base} is independent of joint position and base link orientation, and (iii) off-diagonal elements of I_{base} are negligible. The validity of these strong assumptions in humanoid multi-contact motion is evaluated in Section V-F.

Similar to the linear components, the angular components of centroidal dynamics (1b), under the approximation (6), are represented by the following state equations:

$$\dot{x}_{A*} = \begin{bmatrix} 0 & 1 & 0 \\ 0 & 0 & 1 \\ 0 & 0 & 0 \end{bmatrix} x_{A*} + \begin{bmatrix} 0 \\ 0 \\ 1 \end{bmatrix} u_{A*} \quad (7a)$$

$$y_{A*} = \begin{bmatrix} 1 & 0 & 0 \\ 0 & 0 & I_* \end{bmatrix} x_{A*} \quad (7b)$$

$$\begin{aligned} \text{where } x_{A*} &= [\alpha_* \quad \dot{\alpha}_* \quad \ddot{\alpha}_*]^\top \\ u_{A*} &= \ddot{\alpha}_* \\ y_{A*} &= [\alpha_* \quad \bar{n}_*]^\top \\ * &\in \{x, y, z\} \end{aligned}$$

$\alpha \in \mathbb{R}^3$ is the Euler angle representing the base link orientation. α_* and \bar{n}_* ($* \in \{x, y, z\}$) represent the axis components of α and \bar{n} , respectively. I_* is the diagonal element of I . Although the relation $\omega = K_{\text{Euler}}(\alpha) \dot{\alpha}$ holds, K_{Euler} is ignored in (7). Its validity is evaluated in Section V-F. Compared to the preview control for bipedal walking [21], the proposed method's prominent feature is generating a 6-DoF centroidal trajectory, including position and orientation.

The optimal inputs u_{A*}^{opt} for the same objective function as

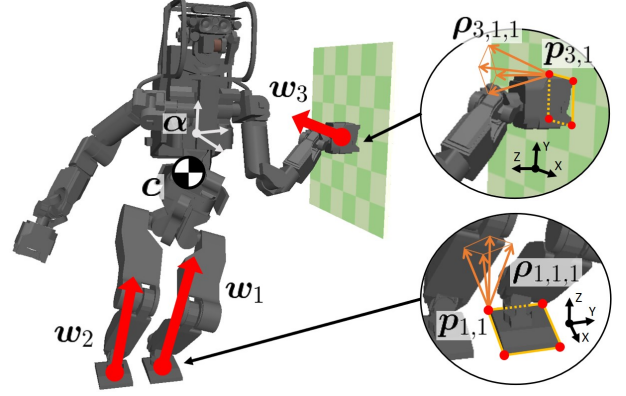


Fig. 2. Contact constraints in wrench distribution.

(4) can be obtained by preview control in the same way as (5).

From the optimal inputs $\ddot{c}^{\text{opt}}, \ddot{\alpha}^{\text{opt}}$, we obtain the planned centroidal state $r^p = [c^{p\top} \quad \alpha^{p\top}]^\top$ and the planned resultant wrench $\bar{w}^p = [\bar{f}^{p\top} \quad \bar{n}^{p\top}]^\top$ by state equations (3) and (7), respectively.

B. Resultant Wrench Projection

1) *Wrench Distribution Formulation*: The resultant wrench \bar{w}^p planned by preview control is not always feasible because the forces the robot receives from the environment are subject to contact constraints. We modify the resultant wrench to be feasible by projecting it onto the constraint manifold defined by the contacts.

The contact wrench at the i -th limb end $w_i = [f_i^\top \quad n_i^\top]^\top$ is represented as follows [19]:

$$w_i = G_i \lambda_i \quad (8)$$

$$\begin{aligned} \text{where } G_i &= \begin{bmatrix} \cdots & \rho_{i,j,k} & \cdots \\ \cdots & \rho_{i,j} \times \rho_{i,j,k} & \cdots \end{bmatrix} \\ \lambda_i &= \begin{bmatrix} \vdots \\ \lambda_{i,j,k} \\ \vdots \end{bmatrix}, \quad \lambda_i \geq 0 \end{aligned}$$

$p_{i,j} \in \mathbb{R}^3$ ($j = 1, \dots, J(i)$) is the j -th vertex of the contact polygon. $\rho_{i,j,k} \in \mathbb{R}^3$ ($k = 1, \dots, K(i,j)$) is the k -th ridge vector of the friction pyramid at the j -th vertex. Fig. 2 illustrates an example of these variables. All variables are

represented in world coordinates. The grasping contacts (e.g., the hand contacts in Fig. 4 (C)) are represented by placing the friction pyramids facing each other.

2) *Wrench Projection*: The contact wrench required to achieve the resultant wrench closest to the planned resultant wrench can be obtained by solving the following QP problem¹:

$$\begin{aligned} \min_{\lambda} \quad & \|G\lambda - w^p\|^2 \quad \text{s.t.} \quad \lambda \geq \mathbf{0} \quad (9) \\ \text{where} \quad & G = [\cdots \quad G_i \quad \cdots] \\ & \lambda = [\cdots \quad \lambda_i^T \quad \cdots]^T \\ & w^p = \bar{w}^p + \begin{bmatrix} mg \\ c^p \times f^p \end{bmatrix} \end{aligned}$$

G is calculated from the target contact state \mathcal{C}^d , which is treated as given, including the contact polygons and friction coefficients.

With λ^{opt} as the optimal variable in (9), the planned resultant wrench projected onto the contact constraint manifold is calculated as follows:

$$\bar{w}^{p'} = G\lambda^{\text{opt}} - \begin{bmatrix} mg \\ c^p \times f^p \end{bmatrix} \quad (10)$$

By inputting $\bar{w}^{p'}$ and integrating (1) for one control period, the desired centroidal state of the next control loop $r^d = [c^d \quad \alpha^d]^T$ is obtained.

IV. CENTROIDAL STABILIZATION CONTROL

A. Centroidal Feedback Control

The stabilizer is responsible for reducing the error between the desired centroidal state r^d and the actual centroidal state r^a based on sensor measurements. We determine the modification amount of the resultant wrench by PD control of the centroidal state as follows:

$$\Delta \bar{w}^d = K_P(r^d - r^a) + K_D(\dot{r}^d - \dot{r}^a) \quad (11a)$$

$$= \begin{bmatrix} K_{P_L}(c^d - c^a) + K_{D_L}(\dot{c}^d - \dot{c}^a) \\ K_{P_A} \log(R^d R^{aT}) + K_{D_A}(\dot{\alpha}^d - \dot{\alpha}^a) \end{bmatrix} \quad (11b)$$

R^d and R^a are the rotation matrices corresponding to α^d and α^a , respectively. $\log(R) \in \mathbb{R}^3$ is a function that converts the rotation matrix R to an equivalent axis-angle vector. Then, the desired resultant wrench is calculated as follows:

$$\bar{w}^d = \bar{w}^{p'} + \Delta \bar{w}^d \quad (12)$$

$K_P, K_D \in \mathbb{R}^{6 \times 6}$ are the diagonal matrices of the feedback gains. We describe the similarity between this control and the bipedal walking control based on the DCM in Appendix-A.

B. Resultant Wrench Distribution

The desired resultant wrench is distributed to the contact wrenches at the limb ends by solving the following QP

problem:

$$\min_{\lambda} \quad \|G\lambda - w^d\|^2 \quad \text{s.t.} \quad \lambda \geq \mathbf{0} \quad (13)$$

$$\text{where} \quad w^d = \bar{w}^d + \begin{bmatrix} mg \\ c^a \times f^d \end{bmatrix}$$

The definitions of G and λ are the same as in (9). From the experimental results in the simulation, it was confirmed that the stability performance is improved by using c^a instead of c^d .

With λ^{opt} as the optimal variable in (13), the desired contact wrench of the i -th limb end is calculated as follows:

$$w_i^d = G_i \lambda_i^{\text{opt}} \quad (14)$$

C. Damping Control for Limb Ends

Damping control [23] is applied to achieve the desired contact wrench w_i^d of each limb end.

Let $p_i^d \in \mathbb{R}^3$ and $R_i^d \in \mathbb{R}^{3 \times 3}$ represent the desired pose of the limb end determined from the given target contact position, and p_i^c and R_i^c represent the compliance pose of the limb end. In damping control, the compliance pose is updated to satisfy the following relationship:

$$K_d \Delta \dot{r}_i^c + K_s \Delta r_i^c = K_f (w_i^a - w_i^d) \quad (15)$$

$$\text{where} \quad \Delta r_i^c = \begin{bmatrix} \Delta r_{i,L}^c \\ \Delta r_{i,A}^c \end{bmatrix} = \begin{bmatrix} p_i^c - p_i^d \\ \log(R_i^c R_i^{dT}) \end{bmatrix}$$

w_i^a is the measured contact wrench at the i -th limb end. We assume that the limb end is equipped with a 6-axis force sensor. $K_d, K_s, K_f \in \mathbb{R}^{6 \times 6}$ are diagonal matrices representing damper parameter, spring parameter, and wrench gain, respectively.

For discrete-time control, (15) is implemented as follows:

$$\Delta r_{i,L}^c[k+1] = \Delta r_{i,L}^c[k] + \Delta t \Delta \dot{r}_{i,L}^c[k] \quad (16a)$$

$$\Delta r_{i,A}^c[k+1] = \log(\exp(\Delta t \Delta \dot{r}_{i,A}^c[k] \times) \exp(\Delta r_{i,A}^c[k] \times)) \quad (16b)$$

$$\text{where} \quad \Delta \dot{r}_i^c[k] = -\frac{K_s}{K_d} \Delta r_i^c[k] + \frac{K_f}{K_d} (w_i^a[k] - w_i^d[k])$$

$\exp(a \times) \in \mathbb{R}^{3 \times 3}$ is a function that converts the axis-angle vector a to an equivalent rotation matrix. Since K_d, K_s, K_f are diagonal matrices, their division implies element-wise computation.

V. SIMULATION EXPERIMENTS

A. Robot Controller Implementation

1) *Software Framework*: The proposed control system is implemented in C++ within a real-time robot control framework `mc_rtc` [24]. QLD [25] is used as the QP solver for wrench distribution. For the preview control, we only need to implement (5), and no external library is required.

Kinematics commands, such as the CoM position and base link orientation r^d and the limb end position and orientation p_i^c, R_i^c , are passed to the acceleration-based whole-body inverse kinematics (IK) calculation. A low stiffness task for nominal joint position is also imposed in IK, so that the joints of the limb without contact approach to the nominal position.

¹To direct the contact force away from the friction cone boundary, a penalty term weighted in the local contact coordinates can be added to the objective function [22].

TABLE I
PARAMETERS FOR PREVIEW CONTROL IN (4) (5)

Q_L	R_L	Q_A	R_A	$\Delta\tau$ [s]	N_h
$\text{diag}(2 \times 10^2, 5 \times 10^{-4})$	$\text{diag}(1 \times 10^{-8})$	$\text{diag}(1 \times 10^2, 5 \times 10^{-3})$	$\text{diag}(1 \times 10^{-8})$	0.005	400(= 2.0/ $\Delta\tau$)

$\Delta\tau$ is the discretization period of the horizon. diag denotes the diagonal matrix.

TABLE II
PARAMETERS FOR DAMPING CONTROL IN (15)

	K_d	K_s	K_f
Contact phase	$\text{diag}(10000, 10000, 10000, 100, 100, 100)$	$\text{diag}(0, 0, 0, 0, 0, 2000)$	$\text{diag}(1, 1, 1, 1, 1, 0)$
Non-contact phase	$\text{diag}(300, 300, 300, 40, 40, 40)$	$\text{diag}(2250, 2250, 2250, 400, 400, 400)$	$\text{diag}(0, 0, 0, 0, 0, 0)$

When K_f is zero, the compliance displacement Δr_i^c converges linearly to zero from (16). When a single limb end is in contact, the parameters of the linear component (the first three elements) of the contacting limb end are set to the parameter values for the non-contact phase. For the linear component of K_d in the contact phase of the hands, different parameter values are used for some motions; 1000 for walking with hands on the wall, and 50000 for climbing a vertical ladder in Fig. 4. The parameter values are different because they are determined to be as compliant as possible within the range of non-vibration, and the hand contact forces, which differ significantly for each motion, affect the ease of vibration.

TABLE III
PARAMETERS FOR CENTROIDAL FEEDBACK CONTROL IN (11)

K_P	K_D
$\text{diag}(2000, 2000, 2000, 0, 0, 0)$	$\text{diag}(666, 666, 666, 0, 0, 0)$

For climbing a vertical ladder in Fig. 4, the following parameters are used:

$$K_P = \text{diag}(3000, 3000, 3000, 1000, 1000, 1000)$$

$$K_D = \text{diag}(1000, 1000, 1000, 333, 333, 333)$$

The calculated joint angles are commanded to the low-level joint position PD controller. As sensor measurements, the proposed control system uses the joint angles from the joint encoders, the contact wrench from the 6-axis force sensors mounted on the hands and feet, and the link orientation from the inertial measurement unit (IMU) sensor mounted on the trunk link.

2) *Controller Parameters*: Tables I, II, and III show the control parameters. For these parameters, the same values are used for bipedal walking and various multi-contact motions presented in this section, except for K_d of hand damping control shown in Table II.

3) *Simulation Environments*: We verified various multi-contact motions of the humanoid robot HRP-5P [26], which is developed by the authors' group, on the dynamics simulator Choreonoid [27]. The control processes shown in Fig. 1 are executed every 2 ms on a single thread with an Intel Core i7-9750H CPU (2.60 GHz) and 32 GB 2667 MHz RAM. We also confirmed that some of the motions can be executed on the dynamics simulator MuJoCo [28] and on other humanoid robots in the HRP series, in order to verify the robustness of the simulation engines and robot models. See the supplemental video for all the experiments.

B. Bipedal Walking

First, the robot performed bipedal walking on uneven floors, stairs, and ramps. Fig. 3 shows the graphs of CoM and ZMP when walking straight on a flat ground with a stride length of 300 mm. The ZMP is not used in the control but is calculated from the resultant wrench for verification only. The reference CoM trajectory is determined by a simple rule; the horizontal

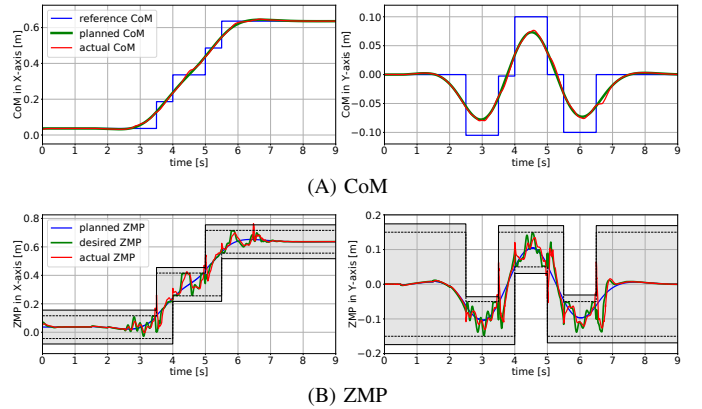


Fig. 3. Results of bipedal walking.

(A) The reference, planned, and actual CoMs correspond to r^{ref} , r^p , and r^a in Fig. 1, respectively. (B) The planned, desired, and actual ZMPs are calculated from w^p , w_i^d , and w_i^a in Fig. 1, respectively. The gray shaded region indicates the support region. The wrench distribution uses contact polygon vertices with inner margins, and the black dashed lines indicate their boundaries.

position is the center of the supporting foot in the single support phase, the center of both feet in the double support phase, and the vertical position is constant. The planned CoM trajectory shown in Fig. 3 (A) is similar to the CoM trajectories planned by the conventional bipedal walking methods [21], although ZMP tracking is not explicitly considered in the proposed method. Fig. 3 (B) shows that the planned ZMP falls within the foot support region, and the ZMP modified by the feedback is tracked by the simulated robot.

C. Multi-contact Motion

We applied the proposed control methods to the five types of multi-contact motions shown in Fig. 4. As shown in the supplemental video, various motions with different contact transition orders, hand forces, and contact forms (i.e., unilateral contact or grasping contact) are stably performed. Figs. 5, 6, and 7 show the graphs of the motion results of Fig. 4 (A), (B), and (C), respectively. It can be observed that the desired contact wrenches distributed to the limb ends are tracked by the damping control, and the simulated robot tracks the

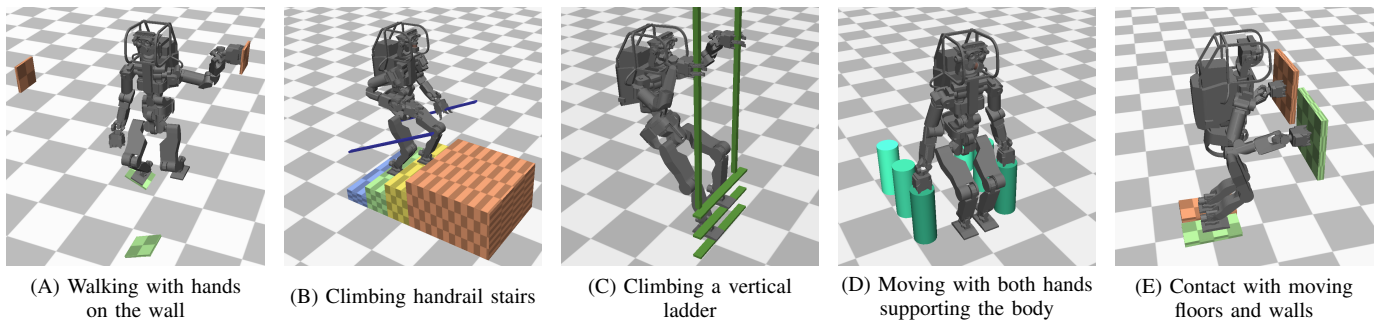


Fig. 4. Simulation of multi-contact motion.

The friction coefficient is set to 0.6 for all environments. (A) Stepping on scaffold boards with 25 degree incline while keeping the hand on a vertical wall. (B) Climbing four steps of 150 mm height with handrails. (C) Climbing a vertical ladder with 200 mm steps. The depth of the ladder rungs is 75 mm, which is less than half the depth of the robot's sole. (D) With both hands on the support surfaces at the height of 500 mm, moving forward by swinging both feet simultaneously. (E) Balancing on the floors and walls, which move periodically in translation and rotation with an amplitude of 20 mm and 2 degrees. Damping control allows feet and hands to adapt to floor and wall movements.

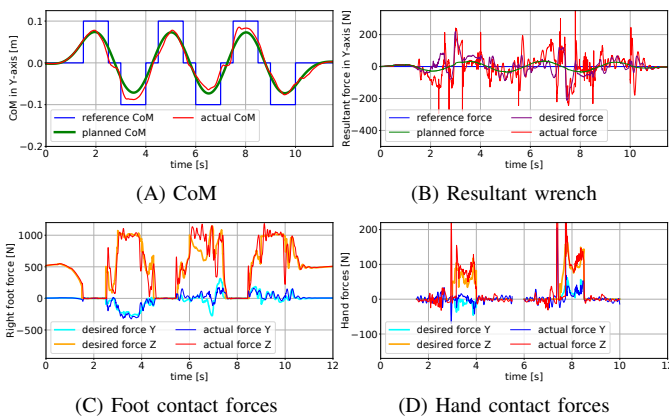


Fig. 5. Results of walking with hands on the wall in Fig. 4 (A).

The CoM and resultant wrench are represented in the world coordinates, and the contact forces are represented in the coordinates at each limb end (see Fig. 2). (B) The reference, planned, desired, and actual resultant forces are calculated from \bar{f}_*^{ref} , \bar{w}^{pl} , w_1^{d} , and w_1^{a} , respectively. (C) The desired and actual forces correspond to w_1^{d} and w_1^{a} , respectively. (D) Contact forces of the left hand (1-6 s) and right hand (6-10 s).

planned CoM trajectory. The reference CoM trajectories are represented by piecewise-constant functions synchronized with the contact switching as Figs. 5, 6, and 7 show. Specifically, in the motions of Fig. 4 (A) and (B), the reference CoM position is determined by the same rule as in bipedal walking described in the previous section. In the motion of Fig. 4 (B), the CoM lateral position in the single support phase is offset inward by 50 mm so that the hands support part of the robot's weight. In the motion of Fig. 4 (C), the reference CoM position is set 0.4 m behind the center of the ladder, but offset forward by 0.1 m to reduce the pitch moment during the hand contact transitions. In all motions, the CoM vertical position is determined by adding a constant offset to the mean of the foot contact positions. The reference base link orientations are all set to zero.

D. Motion to Change the Base Link Orientation

The proposed CoM trajectory generation was applied to a cartwheel motion with a large change in base link orientation, as shown in Fig. 8. From a rough reference centroidal

TABLE IV
COMPUTATION TIME [μs]

	(A)	(B)	(C)
Total control	124	186	409
Calculate reference	22 (18 %)	22 (12 %)	22 (5 %)
Preview control	9 (7 %)	10 (5 %)	9 (2 %)
Project planned wrench	29 (24 %)	56 (30 %)	165 (40 %)
Distribute desired wrench	28 (22 %)	56 (30 %)	162 (40 %)

The computation time per control cycle for the motions (A), (B), and (C) in Fig. 4 is shown. In the computational time measurements, only the proposed centroidal control is included, not the whole-body inverse kinematics. The higher the number of robot contacts, the more time is required for wrench projection and distribution, but the time for the other processes remains almost unchanged.

trajectory and given contact positions, a dynamically feasible centroidal trajectory and contact wrenches are planned such that the base link makes one revolution while moving laterally. Since mapping this centroidal motion to the motion in the joint configuration space is difficult for a simple whole-body inverse kinematics calculation, this paper only verifies the centroidal trajectory generation, and its execution on the robot is out of scope.

E. Computation Time

Table IV shows the computation time of the proposed control method for the multi-contact motions in Fig. 4. It takes 0.1-0.4 ms for one control update, depending on the number of robot contacts. The MPC-based methods take 20 ms for a 3 s horizon (20 sample points) [5] and 1 ms for a 0.5 s horizon (10 sample points) [6] for each control update, whereas our method takes 0.4 ms for a 2 s horizon (400 sample points). This shows that our method reduces the computation time to about half or less while increasing the number of sample points in the horizon by about 20 times.

F. Validation of Rotational Motion Approximation

1) *Approximation of Angular Momentum*: To validate the approximation of the centroidal angular momentum, we calculated the errors between $I_{\text{all}} \dot{q}$, $I_{\text{base}} \omega$, and $I \omega$ in (6) for the motions of bipedal walking and climbing handrail stairs.

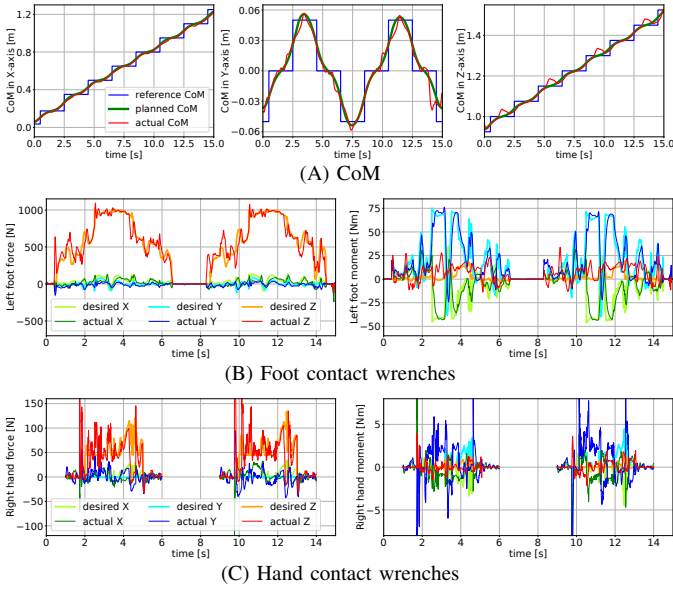


Fig. 6. Results of climbing handrail stairs in Fig. 4 (B). Vertical forces of about 50-100 N are applied to the hands. The error in the Z position of the actual CoM is because the result of the whole-body inverse kinematics cannot follow the desired CoM due to the limitation of kinematics reachability.

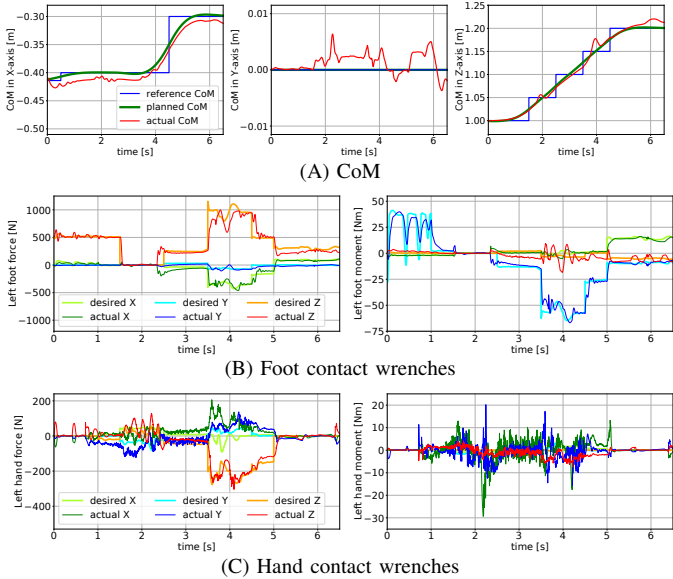


Fig. 7. Results of climbing a vertical ladder in Fig. 4 (C). Pulling forces of about 200 N are applied to the hands. Since the foot is in contact with the ladder rung only at the toes, the foot exerts a large contact moment around the Y-axis.

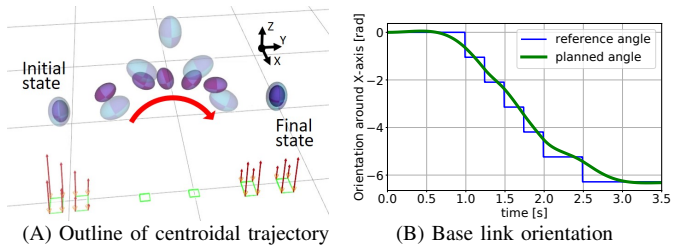


Fig. 8. Centroidal trajectory generation of cartwheel motion. (A) The translucent markers represent the reference, and the non-translucent markers represent the planned centroidal states, respectively. Green rectangles represent the contact positions of the hands and feet.

The mean error was $0.044 \text{ kg m}^2/\text{s}$ for $\|\mathbf{I}_{\text{base}} \boldsymbol{\omega} - \mathbf{I} \boldsymbol{\omega}\|$ and $3.1 \text{ kg m}^2/\text{s}$ for $\|\mathbf{I}_{\text{all}} \dot{\mathbf{q}} - \mathbf{I} \boldsymbol{\omega}\|$. Since the robot did not fall over in the simulation, these errors were not enough to break the motion feasibility. Furthermore, by adding the angular momentum task [1] to the whole-body IK, the mean error was reduced to $0.011 \text{ kg m}^2/\text{s}$ for $\|\mathbf{I}_{\text{all}} \dot{\mathbf{q}} - \mathbf{I} \boldsymbol{\omega}\|$.

2) *Approximation of Angular Velocity*: In (7), the angular velocity of the base link is approximated to the time derivative of the Euler angle. To validate this approximation, we calculated the error between $\mathbf{I} \boldsymbol{\omega}$ and $\mathbf{I} \dot{\boldsymbol{\alpha}}$. The mean error for the same two motions as in the previous section was $0.0051 \text{ kg m}^2/\text{s}$. The small error was due to the small inclination of the base link during the motions. Additionally, the error was small even in the cartwheel motion because $\mathbf{K}_{\text{Euler}}$ was not affected by rotation around the X-axis in the ZYX Euler angle used in our implementation.

G. Comparison with Constrained MPC

The proposed centroidal trajectory generation consists of unconstrained preview control and post-processing wrench projection. This greatly reduces computational cost, but the generated trajectory may be far from the global optimum. We therefore compared the centroidal trajectories generated by the proposed method and the linear MPC-based method [5] for the motions of climbing handrail stairs and climbing a vertical ladder. The mean projection errors of the planned resultant wrench onto the contact constraint manifold (i.e., $\|\bar{\mathbf{w}}^{\text{P}} - \bar{\mathbf{w}}^{\text{P}'}\|$) were 2.2 N and 4.4 Nm for climbing handrail stairs and zero for climbing a vertical ladder in the proposed method. These projection errors were zero in the MPC-based method because the trajectories consistent with the constraints were planned. The mean projection errors of the desired resultant wrench $\bar{\mathbf{w}}^{\text{d}}$ were as follows; for climbing handrail stairs, 3.7 N and 4.7 Nm in the proposed method and 0.42 N and 0.52 Nm in the MPC-based method; and for climbing a vertical ladder, 9.0 N and 8.7 Nm in the proposed method and 9.3 N and 9.1 Nm in the MPC-based method. No significant differences were found in the scale of feedback wrench (11), CoM acceleration, and angular momentum. Based on the above, we conclude that there is no significant difference between the two methods for motions incorporating feedback. Note that the MPC-based method took more than twice as long as the motion duration.

VI. CONCLUSION

In this paper, we proposed a centroidal online trajectory generation and stabilization control for humanoid dynamic multi-contact motion. The controller combines preview control, which does not explicitly consider constraints, with wrench distribution to satisfy contact constraints, and rapidly generates feasible robot motions. Simulation experiments showed that various motions such as bipedal walking and climbing handrail stairs and vertical ladders can be achieved stably by a humanoid robot. The proposed method can update the robot centroidal state in a shorter period for a more finely sampled control horizon than previous methods.

Future works include the online trajectory generation in the joint space in the form of a receding horizon to enhance the

inverse kinematics calculation. This will enable the robot to perform kinematically and dynamically challenging motions such as cartwheels, for which the proposed method generated the centroidal trajectory. Another future direction is to improve the robustness and reliability using a hierarchical scheme that executes the MPC at low periods and the proposed preview control at high periods.

APPENDIX

A. Relationship with DCM-based Bipedal Control

The proportional control of DCM [16], [17] for bipedal walking with constant CoM height and coplanar feet is expressed by the following equation:

$$\mathbf{z}^c = \mathbf{z}^d + \mathbf{K}_\xi(\boldsymbol{\xi}^a - \boldsymbol{\xi}^d) \quad (17)$$

$\mathbf{z} \in \mathbb{R}^2$ is the ZMP, and $\boldsymbol{\xi} \in \mathbb{R}^2$ is the DCM. $\mathbf{K}_\xi \in \mathbb{R}^{2 \times 2}$ is the diagonal matrix of the feedback gain. The superscripts c, d, and a stand for command, desired, and actual, respectively. The command ZMP is converted to the command CoM acceleration and then to the command resultant force as follows:

$$\ddot{\mathbf{c}}^c = \omega^2(\mathbf{c}^d - \mathbf{z}^c) \quad (18a)$$

$$= \ddot{\mathbf{c}}^d + \omega^2 \mathbf{K}_\xi(\boldsymbol{\xi}^d - \boldsymbol{\xi}^a) \quad (18b)$$

$$\mathbf{f}^c = m\ddot{\mathbf{c}}^c \quad (18c)$$

$$= \mathbf{f}^d + m\omega^2 \mathbf{K}_\xi(\mathbf{c}^d - \mathbf{c}^a) + m\omega \mathbf{K}_\xi(\dot{\mathbf{c}}^d - \dot{\mathbf{c}}^a) \quad (18d)$$

$\omega \in \mathbb{R}$ is the LIPM frequency. The LIPM dynamics ($\ddot{\mathbf{c}} = \omega^2(\mathbf{c} - \mathbf{z})$) and the DCM definition ($\boldsymbol{\xi} = \mathbf{c} + \frac{1}{\omega}\dot{\mathbf{c}}$) are used in the equation transformations. (18d) has the same form as the linear part of (11b). The correspondence of the coefficients is as follows:

$$\mathbf{K}_{\text{PL}} = m\omega^2 \mathbf{K}_\xi, \quad \mathbf{K}_{\text{DL}} = m\omega \mathbf{K}_\xi \quad (19)$$

This helps to estimate the feedback gains of (11) in the proposed method. For the HRP-5P, $m = 105$, $\omega^2 = 9.8/0.95 = 10.3$, $\mathbf{K}_\xi = \text{diag}(2, 2)$, and therefore $\mathbf{K}_{\text{PL}} = \text{diag}(2163, 2163)$, $\mathbf{K}_{\text{DL}} = \text{diag}(674, 674)$, which roughly matches the values in Table III.

REFERENCES

- [1] D. E. Orin, A. Goswami, and S.-H. Lee, "Centroidal dynamics of a humanoid robot," *Autonomous Robots*, vol. 35, no. 2, pp. 161–176, 2013.
- [2] H. Dai, A. Valenzuela, and R. Tedrake, "Whole-body motion planning with centroidal dynamics and full kinematics," in *IEEE-RAS International Conference on Humanoid Robots*, 2014, pp. 295–302.
- [3] J. Carpentier and N. Mansard, "Multi-contact locomotion of legged robots," *IEEE Transactions on Robotics*, vol. 34, no. 6, pp. 1441–1460, 2018.
- [4] P. Shah, A. Meduri, W. Merkt, M. Khadiv, I. Havoutis, and L. Righetti, "Rapid convex optimization of centroidal dynamics using block coordinate descent," in *IEEE-RSJ International Conference on Intelligent Robots and Systems*, 2021, pp. 1635–1642.
- [5] H. Audren, J. Vaillant, A. Kheddar, A. Escande, K. Kaneko, and E. Yoshida, "Model preview control in multi-contact motion-application to a humanoid robot," in *IEEE-RSJ International Conference on Intelligent Robots and Systems*, 2014, pp. 4030–4035.
- [6] B. Henze, C. Ott, and M. A. Roa, "Posture and balance control for humanoid robots in multi-contact scenarios based on model predictive control," in *IEEE-RSJ International Conference on Intelligent Robots and Systems*, 2014, pp. 3253–3258.
- [7] S. Caron and A. Kheddar, "Multi-contact walking pattern generation based on model preview control of 3D COM accelerations," in *IEEE-RAS International Conference on Humanoid Robots*, 2016, pp. 550–557.
- [8] P. Fernbach, S. Tonneau, and M. Tax, "CROC: Convex resolution of centroidal dynamics trajectories to provide a feasibility criterion for the multi contact planning problem," in *IEEE-RSJ International Conference on Intelligent Robots and Systems*, 2018, pp. 1–9.
- [9] G. Romualdi, S. Dafarra, G. L'Erario, I. Sorrentino, S. Traversaro, and D. Pucci, "Online non-linear centroidal MPC for humanoid robot locomotion with step adjustment," in *IEEE International Conference on Robotics and Automation*, 2022, pp. 10412–10419.
- [10] M. Morisawa *et al.*, "Sequential trajectory generation for dynamic multi-contact locomotion synchronizing contact," *International Journal of Humanoid Robotics*, vol. 17, no. 1, 2020.
- [11] T. Katayama, T. Ohki, T. Inoue, and T. Kato, "Design of an optimal controller for a discrete-time system subject to previewable demand," *International Journal of Control*, vol. 41, no. 3, pp. 677–699, 1985.
- [12] C. Mastalli, R. Budhiraja, W. Merkt, G. Saurel, B. Hammoud, M. Naveau, J. Carpentier, L. Righetti, S. Vijayakumar, and N. Mansard, "Crocodyl: An efficient and versatile framework for multi-contact optimal control," in *IEEE International Conference on Robotics and Automation*, 2020, pp. 2536–2542.
- [13] C. Ott, M. A. Roa, and G. Hirzinger, "Posture and balance control for biped robots based on contact force optimization," in *IEEE-RAS International Conference on Humanoid Robots*, 2011, pp. 26–33.
- [14] M. Kanazawa, S. Nozawa, Y. Kakiuchi, Y. Kanemoto, M. Kuroda, K. Okada, M. Inaba, and T. Yoshiike, "Robust vertical ladder climbing and transitioning between ladder and catwalk for humanoid robots," in *IEEE-RSJ International Conference on Intelligent Robots and Systems*, 2015, pp. 2202–2209.
- [15] M. P. Polverini, A. Laurenzi, E. M. Hoffman, F. Ruscelli, and N. G. Tsagarakis, "Multi-contact heavy object pushing with a centaur-type humanoid robot: Planning and control for a real demonstrator," *IEEE Robotics and Automation Letters*, vol. 5, no. 2, pp. 859–866, 2020.
- [16] J. Engelsberger, C. Ott, and A. Albu-Schffer, "Three-dimensional bipedal walking control based on divergent component of motion," *IEEE Transactions on Robotics*, vol. 31, no. 2, pp. 355–368, 2015.
- [17] S. Caron, A. Kheddar, and O. Tempier, "Stair climbing stabilization of the hrp-4 humanoid robot using whole-body admittance control," in *IEEE International Conference on Robotics and Automation*, 2019, pp. 277–283.
- [18] S. Kajita, F. Kanehiro, K. Kaneko, K. Yokoi, and H. Hirukawa, "The 3d linear inverted pendulum mode: a simple modeling for a biped walking pattern generation," in *IEEE-RSJ International Conference on Intelligent Robots and Systems*, vol. 1, 2001, pp. 239–246 vol.1.
- [19] K. Bouyarmane, S. Caron, A. Escande, and A. Kheddar, "Multi-contact motion planning and control," in *Humanoid Robotics: A Reference*. Springer, 2018, pp. 1763–1804.
- [20] J. Carpentier, M. Benallegue, N. Mansard, and J.-P. Laumond, "Center-of-mass estimation for a polyarticulated system in contact – a spectral approach," *IEEE Transactions on Robotics*, vol. 32, no. 4, pp. 810–822, 2016.
- [21] S. Kajita, F. Kanehiro, K. Kaneko, K. Fujiwara, K. Harada, K. Yokoi, and H. Hirukawa, "Biped walking pattern generation by using preview control of zero-moment point," in *IEEE International Conference on Robotics and Automation*, vol. 2, 2003, pp. 1620–1626.
- [22] M. Focchi, A. del Prete, I. Havoutis, R. Featherstone, D. G. Caldwell, and C. Semini, "High-slope terrain locomotion for torque-controlled quadruped robots," *Autonomous Robots*, vol. 41, no. 1, pp. 259–272, 2017.
- [23] S. Kajita *et al.*, "Biped walking stabilization based on linear inverted pendulum tracking," in *IEEE-RSJ International Conference on Intelligent Robots and Systems*, 2010, pp. 4489–4496.
- [24] mc_rtc. Accessed: 2021-10-1. [Online]. Available: https://jrl-umi3218.github.io/mc_rtc/
- [25] QLD. Accessed: 2021-10-1. [Online]. Available: https://help.scilab.org/doc/5.5.2/en_US/qld.html
- [26] K. Kaneko, H. Kaminaga, T. Sakaguchi, S. Kajita, M. Morisawa, I. Kumagai, and F. Kanehiro, "Humanoid Robot HRP-5P: An electrically actuated humanoid robot with high-power and wide-range joints," *IEEE Robotics and Automation Letters*, vol. 4, no. 2, pp. 1431–1438, 2019.
- [27] S. Nakaoka, "Choreonoid: Extensible virtual robot environment built on an integrated gui framework," in *IEEE/SICE International Symposium on System Integration*, 2012, pp. 79–85.
- [28] E. Todorov, T. Erez, and Y. Tassa, "MuJoCo: A physics engine for model-based control," in *IEEE-RSJ International Conference on Intelligent Robots and Systems*, 2012, pp. 5026–5033.